Measurements of the branching fractions of
$\eta_c \to K^+K^-\pi^0$, $K_S^0 K^\pm \pi^\mp$, $2(\pi^+\pi^-\pi^0)$, and $p\bar{p}$

M. Ablikim,[1] M. N. Achasov,[10,d] S. Ahmed,[15] M. Albrecht,[4] M. Alekseev,[55a,55c] A. Amoroso,[55a,55c] F. F. An,[1] Q. An,[52,42] Y. Bai,[41] O. Bakina,[27] R. Baldini Ferroli,[23a] Y. Ban,[35] K. Begzsuren,[25] D. W. Bennett,[22] J. V. Bennett,[5] N. Berger,[26] M. Bertani,[23a] D. Bettoni,[24a] F. Bianchi,[55a,55c] J. Bloms,[50] I. Boyko,[27] R. A. Briere,[5] H. Cai,[57] X. Cai,[1,42] A. Calcaterra,[23a] G. F. Cao,[1,46] S. A. Cetin,[45b] J. Chai,[55c] J. F. Chang,[1,42] W. L. Chang,[1,46] G. Chelkov,[27,b,c] G. Chen,[1] H. S. Chen,[1,46] J. C. Chen,[1] M. L. Chen,[1,42] S. J. Chen,[33] Y. B. Chen,[1,42] W. Cheng,[55c] G. Cibinetto,[24a] F. Cossio,[55c] H. L. Dai,[1,42] J. P. Dai,[37,h] A. Dbeyssi,[15] D. Dedovich,[27] Z. Y. Deng,[1] A. Denig,[26] I. Denysenko,[27] M. Destefanis,[55a,55c] F. De Mori,[55a,55c] Y. Ding,[31] C. Dong,[34] J. Dong,[1,42] L. Y. Dong,[1,46] M. Y. Dong,[1,42,46] Z. L. Dou,[33] S. X. Du,[60] J. Z. Fan,[44] J. Fang,[1,42] S. S. Fang,[1,46] Y. Fang,[1] R. Farinelli,[24a,24b] L. Fava,[55b,55c] F. Feldbauer,[4] G. Felici,[23a] C. Q. Feng,[52,42] M. Fritsch,[4] C. D. Fu,[1] Y. Fu,[1] Q. Gao,[1] X. L. Gao,[52,42] Y. Gao,[44] Y. G. Gao,[6] Z. Gao,[52,42] B. Garillon,[26] I. Garzia,[24a] A. Gilman,[49] K. Goetzen,[11] L. Gong,[34] W. X. Gong,[1,42] W. Gradl,[26] M. Greco,[55a,55c] L. M. Gu,[33] M. H. Gu,[1,42] Y. T. Gu,[13] A. Q. Guo,[1,*] L. B. Guo,[32] R. P. Guo,[1,46] Y. P. Guo,[26] A. Guskov,[27] S. Han,[57] X. Q. Hao,[16] F. A. Harris,[47] K. L. He,[1,46] F. H. Heinsius,[4] T. Held,[4] Y. K. Heng,[1,42,46] Z. L. Hou,[1] H. M. Hu,[1,46] J. F. Hu,[37,h] T. Hu,[1,42,46] Y. Hu,[1] G. S. Huang,[52,42] J. S. Huang,[16] X. T. Huang,[36] X. Z. Huang,[33] Z. L. Huang,[31] T. Hussain,[54] N. Hsken,[50] W. Ikegami Andersson,[56] W. Imoehl,[22] M. Irshad,[52,42] Q. Ji,[1] Q. P. Ji,[16] X. B. Ji,[1,46] X. L. Ji,[1,42] H. L. Jiang,[36] X. S. Jiang,[1,42,46] X. Y. Jiang,[34] J. B. Jiao,[36] Z. Jiao,[18] D. P. Jin,[1,42,46] S. Jin,[33] Y. Jin,[48] T. Johansson,[56] N. Kalantar-Nayestanaki,[29] X. S. Kang,[34] M. Kavatsyuk,[29] B. C. Ke,[1] I. K. Keshk,[4] T. Khan,[52,42] A. Khoukaz,[50] P. Kiese,[26] R. Kiuchi,[1] R. Kliemt,[11] L. Koch,[28] O. B. Kolcu,[45b,f] B. Kopf,[4] M. Kuemmel,[4] M. Kuessner,[4] A. Kupsc,[56] M. Kurth,[1] W. Kühn,[28] J. S. Lange,[28] P. Larin,[15] L. Lavezzi,[55c] H. Leithoff,[26] C. Li,[56] Cheng Li,[52,42] D. M. Li,[60] F. Li,[1,42] F. Y. Li,[35] G. Li,[1] H. B. Li,[1,46] H. J. Li,[1,46] J. C. Li,[1] J. W. Li,[40] Ke Li,[1] L. K. Li,[1] Lei Li,[3] P. L. Li,[52,42] P. R. Li,[30] Q. Y. Li,[36] W. D. Li,[1,46] W. G. Li,[1] X. L. Li,[36] X. N. Li,[1,42] X. Q. Li,[34] X. H. Li,[52,42] Z. B. Li,[43] H. Liang,[52,42] Y. F. Liang,[39] Y. T. Liang,[28] G. R. Liao,[12] L. Z. Liao,[1,46] J. Libby,[21] C. X. Lin,[43] D. X. Lin,[15] B. Liu,[37,h] B. J. Liu,[1] C. X. Liu,[1] D. Liu,[52,42] D. Y. Liu,[37,h] F. H. Liu,[38] Fang Liu,[1] Feng Liu,[6] H. B. Liu,[13] H. L. Liu,[41] H. M. Liu,[1,46] Huanhuan Liu,[1] Huihui Liu,[17] J. B. Liu,[52,42] J. Y. Liu,[1,46] K. Y. Liu,[31] Ke Liu,[6] Q. Liu,[46] S. B. Liu,[52,42] X. Liu,[30] Y. B. Liu,[34] Z. A. Liu,[1,42,46] Zhiqing Liu,[26] Y. F. Long,[35] X. C. Lou,[1,42,46] H. J. Lu,[18] J. D. Lu,[1,46] J. G. Lu,[1,42] Y. Lu,[1] Y. P. Lu,[1,42] C. L. Luo,[32] M. X. Luo,[59] P. W. Luo,[43] T. Luo,[9,j] X. L. Luo,[1,42] S. Lusso,[55c] X. R. Lyu,[46] F. C. Ma,[31] H. L. Ma,[1] L. L. Ma,[36] M. M. Ma,[1,46] Q. M. Ma,[1] X. N. Ma,[34,†] X. X. Ma,[1,46] X. Y. Ma,[1,42] Y. M. Ma,[36] F. E. Maas,[15] M. Maggiora,[55a,55c] S. Maldaner,[26] Q. A. Malik,[54] A. Mangoni,[23b] Y. J. Mao,[35] Z. P. Mao,[1] S. Marcello,[55a,55c] Z. X. Meng,[48] J. G. Messchendorp,[29] G. Mezzadri,[24a] J. Min,[1,42] T. J. Min,[33] R. E. Mitchell,[22] X. H. Mo,[1,42,46] Y. J. Mo,[6] C. Morales Morales,[15] N. Yu. Muchnoi,[10,d] H. Muramatsu,[49] A. Mustafa,[4] S. Nakhoul,[11,g] Y. Nefedov,[27] F. Nerling,[11,g] I. B. Nikolaev,[10,d] Z. Ning,[1,42] S. Nisar,[8,k] S. L. Niu,[1,42] S. L. Olsen,[46] Q. Ouyang,[1,42,46] S. Pacetti,[23b] Y. Pan,[52,42] M. Papenbrock,[56] P. Patteri,[23a] M. Pelizaeus,[4] H. P. Peng,[52,42] K. Peters,[11,g] J. Pettersson,[56] J. L. Ping,[32] R. G. Ping,[1,46] A. Pitka,[4] R. Poling,[49] V. Prasad,[52,42] M. Qi,[33] T. Y. Qi,[2] S. Qian,[1,42] C. F. Qiao,[46] N. Qin,[57] X. S. Qin,[4] Z. H. Qin,[1,42] J. F. Qiu,[1] S. Q. Qu,[34] K. H. Rashid,[54,i] C. F. Redmer,[26] M. Richter,[4] M. Ripka,[26] A. Rivetti,[55c] M. Rolo,[55c] G. Rong,[1,46] Ch. Rosner,[15] M. Rump,[50] A. Sarantsev,[27,e] M. Savrié,[24b] K. Schoenning,[56] W. Shan,[19] X. Y. Shan,[52,42] M. Shao,[52,42] C. P. Shen,[2] P. X. Shen,[34] X. Y. Shen,[1,46] H. Y. Sheng,[1] X. Shi,[1,42] X. D. Shi,[52,42] J. J. Song,[36] Q. Q. Song,[52,42] X. Y. Song,[1] S. Sosio,[55a,55c] C. Sowa,[4] S. Spataro,[55a,55c] F. F. Sui,[36] G. X. Sun,[1] J. F. Sun,[16] L. Sun,[57] S. S. Sun,[1,46] X. H. Sun,[1] Y. J. Sun,[52,42] Y. K. Sun,[52,42] Y. Z. Sun,[1] Z. J. Sun,[1,42] Z. T. Sun,[1] Y. T. Tan,[52,42] C. J. Tang,[39] G. Y. Tang,[1] X. Tang,[1] B. Tsednee,[25] I. Uman,[45d] B. Wang,[1] B. L. Wang,[46] C. W. Wang,[33] D. Y. Wang,[35] H. H. Wang,[36] K. Wang,[1,42] L. L. Wang,[1] L. S. Wang,[1] M. Wang,[36] Meng Wang,[1,46] P. Wang,[1] P. L. Wang,[1] R. M. Wang,[58] W. P. Wang,[52,42] X. Wang,[35] X. F. Wang,[1] Y. Wang,[52,42] Y. F. Wang,[1,42,46] Z. Wang,[1,42] Z. G. Wang,[1,42] Z. Y. Wang,[1] Zongyuan Wang,[1,46] T. Weber,[4] D. H. Wei,[12] P. Weidenkaff,[26] S. P. Wen,[1] U. Wiedner,[4] M. Wolke,[56] L. H. Wu,[1] L. J. Wu,[1,46] Z. Wu,[1,42] L. Xia,[52,42] Y. Xia,[20] Y. J. Xiao,[1,46] Z. J. Xiao,[32] Y. G. Xie,[1,42] Y. H. Xie,[6] X. A. Xiong,[1,46] Q. L. Xiu,[1,42] G. F. Xu,[1] L. Xu,[1] Q. J. Xu,[14] W. Xu,[1,46] X. P. Xu,[40] F. Yan,[53] L. Yan,[55a,55c] W. B. Yan,[52,42] W. C. Yan,[2] Y. H. Yan,[20] H. J. Yang,[37,h] H. X. Yang,[1] L. Yang,[57] R. X. Yang,[52,42] S. L. Yang,[1,46] Y. H. Yang,[33] Y. X. Yang,[12] Yifan Yang,[1,46] Z. Q. Yang,[20] M. Ye,[1,42] M. H. Ye,[7] J. H. Yin,[1] Z. Y. You,[43] B. X. Yu,[1,42,46] C. X. Yu,[34] J. S. Yu,[20] C. Z. Yuan,[1,46] Y. Yuan,[1] A. Yuncu,[45b,a] A. A. Zafar,[54] Y. Zeng,[20] B. X. Zhang,[1] B. Y. Zhang,[1,42] C. C. Zhang,[1] D. H. Zhang,[1] H. H. Zhang,[43] H. Y. Zhang,[1,42] J. Zhang,[1,46] J. L. Zhang,[58] J. Q. Zhang,[4] J. W. Zhang,[1,42,46] J. Y. Zhang,[1] J. Z. Zhang,[1,46] K. Zhang,[1,46] L. Zhang,[44] S. F. Zhang,[33] T. J. Zhang,[37,h] X. Y. Zhang,[36] Y. Zhang,[52,42] Y. H. Zhang,[1,42] Y. T. Zhang,[52,42] Yang Zhang,[1] Yao Zhang,[1] Yu Zhang,[46] Z. H. Zhang,[6] Z. P. Zhang,[52] Z. Y. Zhang,[57] G. Zhao,[1] J. W. Zhao,[1,42] J. Y. Zhao,[1,46] J. Z. Zhao,[1,42] Lei Zhao,[52,42] Ling Zhao,[1] M. G. Zhao,[34] Q. Zhao,[1] S. J. Zhao,[60] T. C. Zhao,[1] Y. B. Zhao,[1,42] Z. G. Zhao,[52,42] A. Zhemchugov,[27,b] B. Zheng,[53] J. P. Zheng,[1,42] Y. Zheng,[35] Y. H. Zheng,[46] B. Zhong,[32] L. Zhou,[1,42] Q. Zhou,[1,46] X. Zhou,[57] X. K. Zhou,[52,42]

X. R. Zhou,[52,42] Xiaoyu Zhou,[20] Xu Zhou,[20] A. N. Zhu,[1,46] J. Zhu,[34] J. Zhu,[43] K. Zhu,[1] K. J. Zhu,[1,42,46] S. H. Zhu,[51] X. L. Zhu,[44] Y. C. Zhu,[52,42] Y. S. Zhu,[1,46] Z. A. Zhu,[1,46] J. Zhuang,[1,42] B. S. Zou,[1] and J. H. Zou[1]

(BESIII Collaboration)

[1]*Institute of High Energy Physics, Beijing 100049, People's Republic of China*
[2]*Beihang University, Beijing 100191, People's Republic of China*
[3]*Beijing Institute of Petrochemical Technology, Beijing 102617, People's Republic of China*
[4]*Bochum Ruhr-University, D-44780 Bochum, Germany*
[5]*Carnegie Mellon University, Pittsburgh, Pennsylvania 15213, USA*
[6]*Central China Normal University, Wuhan 430079, People's Republic of China*
[7]*China Center of Advanced Science and Technology, Beijing 100190, People's Republic of China*
[8]*COMSATS University Islamabad, Lahore Campus, Defence Road, Off Raiwind Road,
54000 Lahore, Pakistan*
[9]*Fudan University, Shanghai 200443, People's Republic of China*
[10]*G.I. Budker Institute of Nuclear Physics SB RAS (BINP), Novosibirsk 630090, Russia*
[11]*GSI Helmholtzcentre for Heavy Ion Research GmbH, D-64291 Darmstadt, Germany*
[12]*Guangxi Normal University, Guilin 541004, People's Republic of China*
[13]*Guangxi University, Nanning 530004, People's Republic of China*
[14]*Hangzhou Normal University, Hangzhou 310036, People's Republic of China*
[15]*Helmholtz Institute Mainz, Johann-Joachim-Becher-Weg 45, D-55099 Mainz, Germany*
[16]*Henan Normal University, Xinxiang 453007, People's Republic of China*
[17]*Henan University of Science and Technology, Luoyang 471003, People's Republic of China*
[18]*Huangshan College, Huangshan 245000, People's Republic of China*
[19]*Hunan Normal University, Changsha 410081, People's Republic of China*
[20]*Hunan University, Changsha 410082, People's Republic of China*
[21]*Indian Institute of Technology Madras, Chennai 600036, India*
[22]*Indiana University, Bloomington, Indiana 47405, USA*
[23a]*INFN Laboratori Nazionali di Frascati, I-00044, Frascati, Italy*
[23b]*INFN and University of Perugia, I-06100, Perugia, Italy*
[24a]*INFN Sezione di Ferrara, I-44122, Ferrara, Italy*
[24b]*University of Ferrara, I-44122, Ferrara, Italy*
[25]*Institute of Physics and Technology, Peace Ave. 54B, Ulaanbaatar 13330, Mongolia*
[26]*Johannes Gutenberg University of Mainz, Johann-Joachim-Becher-Weg 45, D-55099 Mainz, Germany*
[27]*Joint Institute for Nuclear Research, 141980 Dubna, Moscow region, Russia*
[28]*Justus-Liebig-Universitaet Giessen, II. Physikalisches Institut, Heinrich-Buff-Ring 16,
D-35392 Giessen, Germany*
[29]*KVI-CART, University of Groningen, NL-9747 AA Groningen, The Netherlands*
[30]*Lanzhou University, Lanzhou 730000, People's Republic of China*
[31]*Liaoning University, Shenyang 110036, People's Republic of China*
[32]*Nanjing Normal University, Nanjing 210023, People's Republic of China*
[33]*Nanjing University, Nanjing 210093, People's Republic of China*
[34]*Nankai University, Tianjin 300071, People's Republic of China*
[35]*Peking University, Beijing 100871, People's Republic of China*
[36]*Shandong University, Jinan 250100, People's Republic of China*
[37]*Shanghai Jiao Tong University, Shanghai 200240, People's Republic of China*
[38]*Shanxi University, Taiyuan 030006, People's Republic of China*
[39]*Sichuan University, Chengdu 610064, People's Republic of China*
[40]*Soochow University, Suzhou 215006, People's Republic of China*
[41]*Southeast University, Nanjing 211100, People's Republic of China*
[42]*State Key Laboratory of Particle Detection and Electronics, Beijing 100049,
Hefei 230026, People's Republic of China*
[43]*Sun Yat-Sen University, Guangzhou 510275, People's Republic of China*
[44]*Tsinghua University, Beijing 100084, People's Republic of China*
[45a]*Ankara University, 06100 Tandogan, Ankara, Turkey*
[45b]*Istanbul Bilgi University, 34060 Eyup, Istanbul, Turkey*
[45c]*Uludag University, 16059 Bursa, Turkey*
[45d]*Near East University, Nicosia, North Cyprus, Mersin 10, Turkey*
[46]*University of Chinese Academy of Sciences, Beijing 100049, People's Republic of China*
[47]*University of Hawaii, Honolulu, Hawaii 96822, USA*

[48]*University of Jinan, Jinan 250022, People's Republic of China*
[49]*University of Minnesota, Minneapolis, Minnesota 55455, USA*
[50]*University of Muenster, Wilhelm-Klemm-Str. 9, 48149 Muenster, Germany*
[51]*University of Science and Technology Liaoning, Anshan 114051, People's Republic of China*
[52]*University of Science and Technology of China, Hefei 230026, People's Republic of China*
[53]*University of South China, Hengyang 421001, People's Republic of China*
[54]*University of the Punjab, Lahore-54590, Pakistan*
[55a]*University of Turin, I-10125, Turin, Italy*
[55b]*University of Eastern Piedmont, I-15121, Alessandria, Italy*
[55c]*INFN, I-10125, Turin, Italy*
[56]*Uppsala University, Box 516, SE-75120 Uppsala, Sweden*
[57]*Wuhan University, Wuhan 430072, People's Republic of China*
[58]*Xinyang Normal University, Xinyang 464000, People's Republic of China*
[59]*Zhejiang University, Hangzhou 310027, People's Republic of China*
[60]*Zhengzhou University, Zhengzhou 450001, People's Republic of China*

Using data samples collected with the BESIII detector at center-of-mass energies $\sqrt{s} = 4.23, 4.26, 4.36,$ and 4.42 GeV, we measure the branching fractions of $\eta_c \to K^+K^-\pi^0$, $K_S^0 K^\pm \pi^\mp$, $2(\pi^+\pi^-\pi^0)$, and $p\bar{p}$, via the process $e^+e^- \to \pi^+\pi^- h_c$, $h_c \to \gamma\eta_c$. The corresponding results are $(1.15 \pm 0.12 \pm 0.10)\%$, $(2.60 \pm 0.21 \pm 0.20)\%$, $(15.2 \pm 1.8 \pm 1.7)\%$, and $(0.120 \pm 0.026 \pm 0.015)\%$, respectively. Here the first uncertainties are statistical, and the second ones systematic. Additionally, the charged track multiplicity of η_c decays is measured for the first time.

*Corresponding author.
guoaq@ihep.ac.cn
†Corresponding author.
zimeng@mail.nankai.edu.cn
[a]Also at Bogazici University, 34342 Istanbul, Turkey.
[b]Also at the Moscow Institute of Physics and Technology, Moscow 141700, Russia.
[c]Also at the Functional Electronics Laboratory, Tomsk State University, Tomsk, 634050, Russia.
[d]Also at the Novosibirsk State University, Novosibirsk, 630090, Russia.
[e]Also at the NRC "Kurchatov Institute", PNPI, 188300, Gatchina, Russia.
[f]Also at Istanbul Arel University, 34295 Istanbul, Turkey.
[g]Also at Goethe University Frankfurt, 60323 Frankfurt am Main, Germany.
[h]Also at Key Laboratory for Particle Physics, Astrophysics and Cosmology, Ministry of Education; Shanghai Key Laboratory for Particle Physics and Cosmology; Institute of Nuclear and Particle Physics, Shanghai 200240, People's Republic of China.
[i]Also at Government College Women University, Sialkot - 51310. Punjab, Pakistan.
[j]Also at Key Laboratory of Nuclear Physics and Ion-beam Application (MOE) and Institute of Modern Physics, Fudan University, Shanghai 200443, People's Republic of China.
[k]Also at Harvard University, Department of Physics, Cambridge, Massachusetts, 02138, USA.

I. INTRODUCTION

Many new charmonium or charmoniumlike states have been discovered recently [1], which broaden our horizon on understanding the charmonium family. These states have led to a revived interest in improving the quark-model picture of hadrons. However, the knowledge of the lowest lying charmonium state, η_c, is relatively poor compared to other charmonium states. The reason is that most of the measurements involving η_c were performed using the magnetic dipole ($M1$) transitions from J/ψ or hindered $M1$ transitions from $\psi(3686)$. In these decays, the interference between η_c and non-η_c amplitudes affects the η_c line shape [2]. The branching fraction (BF) of η_c decays and the $M1$ transition rate are entangled. The insufficient understanding of the η_c properties has so far prevented precise studies of η_c decays themselves or of decays involving the η_c. For example, in 2002, the Belle Collaboration released the measurements on the total cross section of the exclusive production of $J/\psi + \eta_c$ via the e^+e^- annihilation at the center-of-mass collision energy $\sqrt{s} = 10.58$ GeV [3] with the result of $\sigma[e^+e^- \to J/\psi + \eta_c] \times \mathrm{BF}(\eta_c \to \geq 4 \text{ charged}) = 33^{+7}_{-6} \pm 9$ fb. These measurements were improved as $\sigma[e^+e^- \to J/\psi\eta_c(\gamma)] \times \mathrm{BF}(\eta_c \to \geq 2 \text{ charged}) = 25.6 \pm 2.8 \pm 3.4$ fb [4]. In 2005, the *BABAR* Collaboration independently measured the total cross section as $17.6 \pm 2.8^{+1.5}_{-2.1}$ fb [5]. As the number of charged tracks is required in these measurements, the results will be improved if the charged tracks multiplicity is fully studied.

Recently, the electric dipole (E1) transition $h_c \to \gamma \eta_c$ was found to be a perfect process to measure both η_c resonant parameters and its decay BFs [6]. In addition, the h_c production proceeds via $\psi(3686) \to \pi^0 h_c$, where the interference effect between η_c and non-η_c is much less than that in $J/\psi, \psi(3686)$ radiative transition. One can draw such a conclusion according to the following calculation. The E1 transition rate, BF($h_c \to \gamma \eta_c$) = 50%, is about 2 orders of magnitude larger than that of the M1 transition BF($\psi(3686) \to \gamma \eta_c$) = 0.3% [7]. On the other hand, the background that can interfere with the signal comes from charmonium radiative decays, e.g., h_c, $\psi(3686) \to \gamma +$ hadrons. If we assume the radiative decay rates of h_c and $\psi(3686)$ to be at the same level, therefore, this kind of background in the process $h_c \to \gamma \eta_c$ should be 1 to 2 orders of magnitude less than in $\psi(3686) \to \gamma \eta_c$.

BESIII has collected sizable data samples between 4.009 and 4.600 GeV (called "XYZ data" hereafter) since 2013 to study the XYZ states [8]. A large production rate of $e^+ e^- \to \pi^+ \pi^- h_c$ has been found [9]. The total number of h_c events in all these data samples combined is comparable to that from $\psi(3686) \to \pi^0 h_c$ decays in BESIII data, according to the measured cross section and the corresponding integrated luminosity at each energy point. The h_c is tagged by the recoil mass (RM) of $\pi^+ \pi^-$ in XYZ data, while it is tagged by the recoil mass of π^0 in $\psi(3686)$ data. Generally, the two-charged-pion mode has lower background and higher detection efficiency than the neutral pion mode.

In this paper, we report a measurement of the BFs of four η_c exclusive decays via the process $e^+ e^- \to \pi^+ \pi^- h_c$, $h_c \to \gamma \eta_c$. These exclusive decays are $\eta_c \to K^+ K^- \pi^0$, $K_S^0 K^\pm \pi^\mp$, $2(\pi^+ \pi^- \pi^0)$, and $p \bar{p}$, respectively.

Apart from the BF measurement mentioned above, we also measure the charged tracks multiplicities in inclusive η_c decays by using an unfolding method [10].

II. METHODOLOGY

The BFs of η_c exclusive decays are obtained by a simultaneous fit to the RM spectrum of $\pi^+ \pi^- \gamma$ for both inclusive and exclusive modes. The BFs are common parameters independent of the center of mass energy. The numbers of the η_c signal events of the exclusive and inclusive decay modes can be calculated by the following formulas,

$$N_{\text{exclusive}}^i = \mathcal{L}^i \times \sigma^i(e^+ e^- \to \pi^+ \pi^- h_c) \times \text{BF}(h_c \to \gamma \eta_c) \times \text{BF}(\eta_c \to X) \times \text{BF}(X \to Y) \times \epsilon_{\text{exclusive}}^i, \tag{1}$$

and

$$N_{\text{inclusive}}^i = \mathcal{L}^i \times \sigma^i(e^+ e^- \to \pi^+ \pi^- h_c) \times \text{BF}(h_c \to \gamma \eta_c) \times \epsilon_{\text{inclusive}}^i, \tag{2}$$

where the subscript i denotes the different center-of-mass energy points. $\mathcal{L}$ and σ denote the luminosity and cross section, respectively. X denotes a certain η_c exclusive decay mode, Y denotes the possible π^0 or K_S^0 final state from X decay. ϵ denotes the detection efficiency determined by Monte Carlo (MC) simulations.

By comparing Eq. (1) and Eq. (2), BF($\eta_c \to X$) can be extracted as

$$\text{BF}(\eta_c \to X) = \frac{N_{\text{exclusive}}^i / (\text{BF}(X \to Y) \times \epsilon_{\text{exclusive}}^i)}{N_{\text{inclusive}}^i / \epsilon_{\text{inclusive}}^i}. \tag{3}$$

In the simultaneous fit, the total number of free parameters is less than in the fits taken individually, due to common parameters such as the η_c mass and width, *etc.* In addition, some parameters, for example, $\sigma(e^+ e^- \to \pi^+ \pi^- h_c)$, $\mathcal{L}$, are not necessary in the measurement according to Eq. (3), resulting in reduced statistical uncertainties. In addition, systematic uncertainties from the same sources, e.g., the tracking efficiency of two pions from $e^+ e^- \to \pi^+ \pi^- h_c$, can be canceled.

III. DETECTOR AND DATA SAMPLES

The BESIII detector is a magnetic spectrometer [11] located at the Beijing Electron Positron Collider (BEPCII) [12]. The cylindrical core of the BESIII detector consists of a helium-based multilayer drift chamber (MDC), a plastic scintillator time-of-flight system (TOF), and a CsI(Tl) electromagnetic calorimeter (EMC), which are all enclosed in a superconducting solenoidal magnet providing a 1.0 T magnetic field. The solenoid is supported by an octagonal flux-return yoke with resistive plate counter muon identifier modules interleaved with steel. The acceptance of charged particles and photons is 93% over a 4π solid angle. The charged-particle momentum resolution at 1 GeV/c is 0.5%, and the specific energy loss (dE/dx) resolution is 6% for the electrons from Bhabha scattering. The EMC measures photon energies with a resolution of 2.5% (5%) at 1 GeV in the barrel (end cap) region. The time resolution of the TOF barrel part is 68 ps, while that of the end cap part is 110 ps.

The data samples collected at four center-of-mass energies, i.e., $\sqrt{s} = 4.23$, 4.26, 4.36, and 4.42 GeV [8], are used for our studies. Simulated samples produced with the GEANT4-based [13] MC package which includes the

geometric description of the BESIII detector and the detector response, are used to determine the detection efficiency and to estimate the backgrounds. The simulation includes the beam energy spread and initial state radiation (ISR) in the e^+e^- annihilations modeled with the generator KKMC [14].

The inclusive MC samples have the equivalent luminosities the same as the data samples. They consist of the production of open charm processes, the ISR production of vector charmonium(like) states, and the continuum processes incorporated in KKMC [14]. The known decay modes (∼50%) are modeled with EVTGEN [15] using branching fractions taken from PDG [7], and the remaining unknown decays (∼50%) from the charmonium states with LUNDCHARM [16]. The final state radiations (FSR) from charged final state particles are incorporated with the PHOTOS package [17].

Signal MC samples with 200 000 events each are generated for each η_c decay mode (inclusive and exclusive decays) at each center-of-mass energy. ISR is simulated using KKMC with a maximum energy for the ISR photon corresponding to the $\pi^+\pi^-h_c$ mass threshold. The $E1$ transition $h_c \to \gamma\eta_c$ is generated with an angular distribution of $1 + \cos^2\theta$, where θ is the angle of the $E1$ photon with respect to the h_c helicity direction in the h_c rest frame. The inclusive decays of η_c are produced similarly to the inclusive MC samples.

IV. EVENT SELECTIONS

In this analysis, the η_c signal is tagged with $RM(\pi^+\pi^-\gamma)$ by requiring $RM(\pi^+\pi^-)$ in h_c signal region. For the inclusive mode, at least two charged tracks and one photon is required. For the exclusive modes, the requirements on charged tracks and photon candidates depend on their respective final state.

Charged tracks at BESIII are reconstructed from MDC hits within a polar-angle (θ) acceptance range of $|\cos\theta| < 0.93$. We require that these tracks pass within 10 cm of the interaction point in the beam direction and

within 1 cm in the plane perpendicular to the beam. Tracks used in reconstructing K_S^0 decays are exempted from these requirements.

A vertex fit constrains charged tracks to a common production vertex, which is updated on a run-by-run basis. For each charged track, TOF and dE/dx information is combined to compute particle identification (PID) confidence levels for the pion, kaon, and proton hypotheses.

Electromagnetic showers are reconstructed by clustering EMC crystal energies. Efficiency and energy resolution are improved by including energy deposits in nearby TOF counters. A photon candidate is defined as an isolated shower with an energy deposit of at least 25 MeV in the barrel region ($|\cos\theta| < 0.8$), or of at least 50 MeV in the end cap region ($0.86 < |\cos\theta| < 0.92$). Showers in the transition region between the barrel and the end cap are not well measured and are rejected. An additional requirement on the EMC hit timing suppresses electronic noise and energy deposits unrelated to the event.

A candidate π^0 is reconstructed from pairs of photons with an invariant mass in the range $|M_{\gamma\gamma} - m_{\pi^0}| < 15$ MeV/c^2 [7]. A one-constraint (1C) kinematic fit is performed to improve the energy resolution, with the $M_{\gamma\gamma}$ constrained to the known π^0 mass.

We reconstruct $K_S^0 \to \pi^+\pi^-$ candidates using pairs of oppositely charged tracks with an invariant mass in the range $|M_{\pi^+\pi^-} - m_{K_S^0}| < 20$ MeV/c^2, where $m_{K_S^0}$ is the known K_S^0 mass [7]. To reject random $\pi^+\pi^-$ combinations, a secondary-vertex fitting algorithm is employed to impose the kinematic constraint between the production and decay vertices [18]. Accepted K_S^0 candidates are required to have a decay length of at least twice the vertex resolution. If there is more than one $\pi^+\pi^-$ combinations in an events, the one with the smallest χ^2 of the secondary vertex fit is retained.

In selecting the candidates of the η_c inclusive decay, all charged tracks are assumed to be pions, and events with at least one combination satisfying $RM(\pi^+\pi^-) \in [3.46, 3.59]$ GeV/c^2 and $RM(\pi^+\pi^-\gamma) \in [2.52, 3.4]$ GeV/c^2 are kept
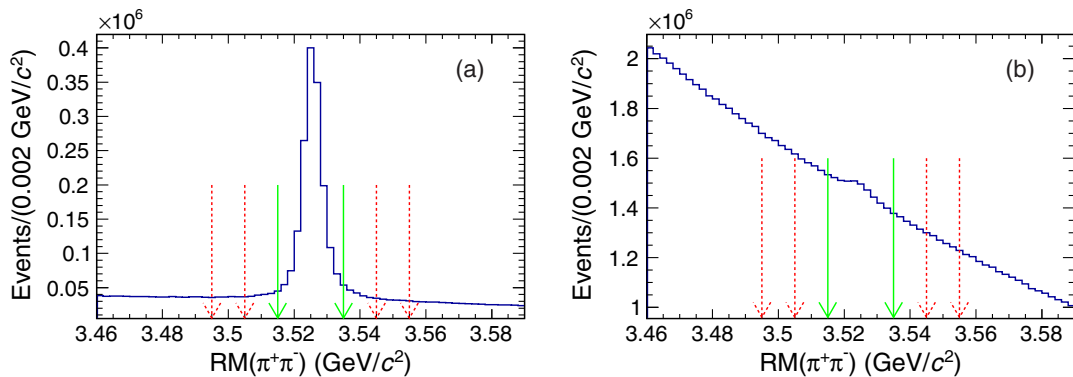

FIG. 1.   Distribution of $RM(\pi^+\pi^-)$ of the η_c inclusive decay from signal MC simulation (a) and data (b) summed over all the four center-of-mass energies. The h_c signal and sideband regions are marked by the solid and dashed arrows, respectively.

TABLE I. Requirements of the number of photons, charged tracks, π^0, and K_S^0 candidates in exclusive η_c decay modes, denoted as N_{charge}, N_γ, N_{π^0}, and $N_{K_S^0}$, respectively.

Decay mode	N_{charge}	N_γ	Other requirements
$\eta_c \to K^+ K^- \pi^0$	$=2$	≥ 3	$N_{\pi^0} \geq 1$
$\eta_c \to K_S^0 K^\pm \pi^\mp$	$=4$	≥ 1	$N_{K_S^0} = 1$
$\eta_c \to 2(\pi^+\pi^-\pi^0)$	$=4$	≥ 5	$N_{\pi^0} \geq 2$
$\eta_c \to p\bar{p}$	$=2$	≥ 1	$\cdots$

TABLE II. The requirements of χ_{4C}^2 for the exclusive decays of η_c.

$\sqrt{s}$ (GeV)	$K_S^0 K^\pm \pi^\mp$	$K^+ K^- \pi^0$	$2(\pi^+\pi^-\pi^0)$	$p\bar{p}$
4.23	45	25	35	40
4.26	45	15	30	40
4.36	45	25	25	40
4.42	50	20	35	40

for further analysis. The region satisfying $RM(\pi^+\pi^-) \in [3.515, 3.535]$ GeV/c^2 is taken as the h_c signal region, while the regions satisfying $RM(\pi^+\pi^-) \in [3.495, 3.505]$ GeV/c^2 or $RM(\pi^+\pi^-) \in [3.545, 3.555]$ GeV/c^2 are taken as the h_c sidebands region. Figure 1 shows the distribution of $RM(\pi^+\pi^-)$ for all $\pi^+\pi^-$ combinations from the inclusive decay mode in signal MC simulations and data (summed over four center-of-mass energies), respectively.

For the selection of exclusive η_c decays, the requirements on the number of photons and charged tracks are listed in Table I. A four-constraint (4C) kinematic fit imposing overall energy-momentum conservation is performed. To determine the species of final state particles and to select the best combination when additional photons (or π^0 candidates) are found in an event, the combination with the minimum value of $\chi^2 = \chi_{4C}^2 + \chi_{1C}^2 + \sum_{i=1}^{N_{\text{charge}}} \chi_{\text{PID}}^2 + \chi_{\text{Vertex}}^2$ is selected for further analysis, where χ_{4C}^2 is the χ^2 from the four-momentum conservation kinematic fit and

χ_{1C}^2 is the sum of the 1C (mass constraint of the two daughter photons) χ^2 of the π^0 in the final state. χ_{PID}^2 is the χ^2 from the PID of different particle hypothesis, using the energy loss in the MDC and the time measured with the TOF system, N_{charge} is the number of the charged tracks in the final states. χ_{Vertex}^2 is the χ^2 of the vertex fit in K_S^0 reconstruction. The χ_{4C}^2 is required to be not more than 50 depending on the η_c decay modes, which is optimized using the figure of merit $N_S/\sqrt{N_S + N_B}$, where N_S is the number of signal events obtained from MC simulation (normalized to data luminosity), while N_B is the number of background events obtained from the sidebands of h_c in data. The requirement on χ_{4C}^2 for the different exclusive decay modes are listed in Table II. In addition, we require the same h_c mass windows on the $RM(\pi^+\pi^-)$ spectra for both inclusive and exclusive modes.

V. NUMERICAL RESULTS OF BF($\eta_c \to X$)

A simultaneous unbinned maximum likelihood fit to the $RM(\pi^+\pi^-\gamma)$ spectrum of the exclusive decays and the inclusive decay of η_c at the four center-of-mass energies is performed to obtain the branching fractions BF($\eta_c \to X$). The fit function is parametrized as follows:

$$F(M) = \sigma \otimes [\epsilon(M) \times |BW(M)|^2 \times E_\gamma^3 \times f_d(E_\gamma)] + B(M),$$

(4)

where the signal function is described by a Breit-Wigner function, $BW(M)$, convolved with the detection resolution, σ. The mass and width of $BW(M)$ are fixed to the η_c nominal values taken from the PDG [7]. M represents the recoil mass $RM(\pi^+\pi^-\gamma)$. The detection resolution is described by a double Gaussian function, whose parameters are obtained from MC simulations. $\epsilon(M)$ is the efficiency curve, obtained from a fit of the efficiencies along the $RM(\pi^+\pi^-\gamma)$ spectrum with a polynomial function and fixed in the fit to data. Figure 2 shows the efficiencies along the $RM(\pi^+\pi^-\gamma)$ spectrum for the inclusive η_c decay and the exclusive decay $\eta_c \to K^+K^-\pi^0$ at $\sqrt{s} = 4.23$ GeV.

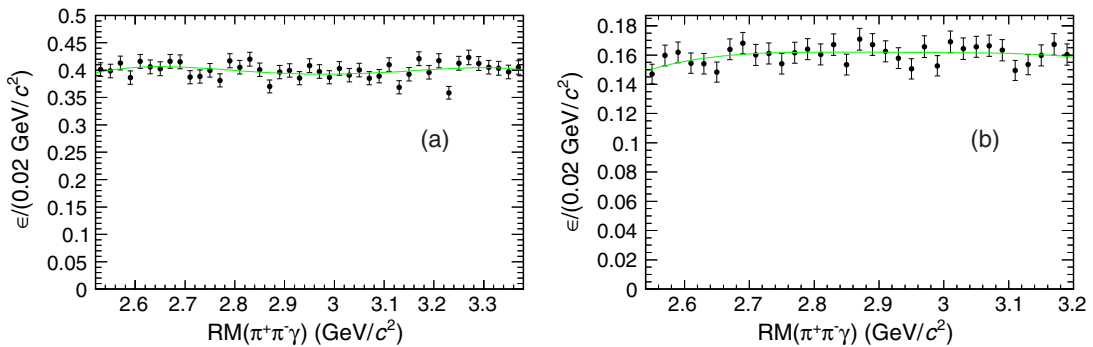

FIG. 2. Efficiencies along the $RM(\pi^+\pi^-\gamma)$ spectra from MC simulation at $\sqrt{s} = 4.23$ GeV for inclusive decay (a) and $\eta_c \to K^+K^-\pi^0$ (b). The curves are the fit results.
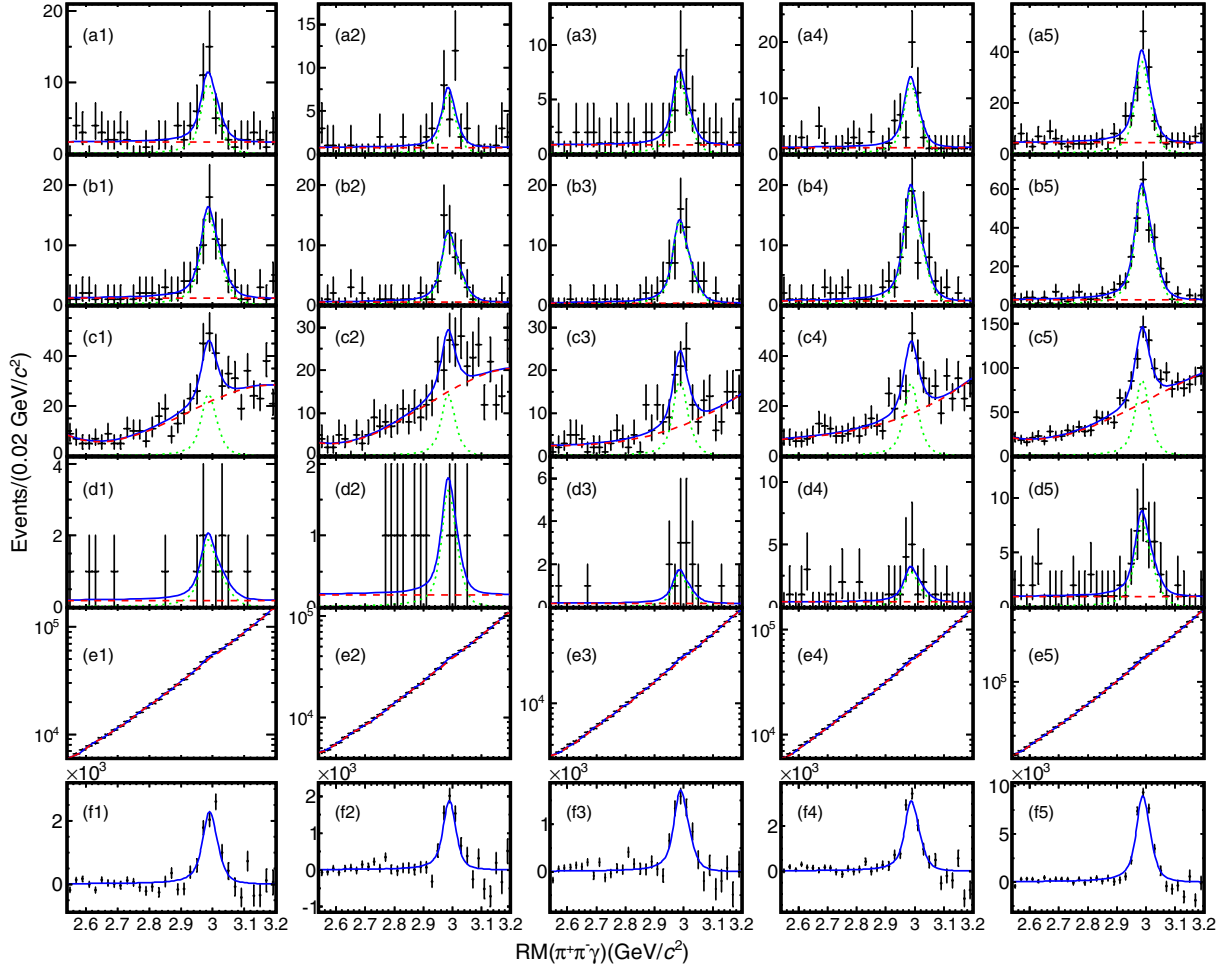
FIG. 3. Projections of the simultaneous fit to data. The dots with error bars denote data, the dashed lines denote backgrounds, the dotted lines denote signals, and the solid lines are the fitting curve. The columns from left to right, labeled from (1) to (5), denote $\sqrt{s} = 4.23$, 4.26, 4.36, 4.42 GeV, and the sum, while the rows from (a) to (d) show the four exclusive decay modes of η_c, namely, $\eta_c \to K^+K^-\pi^0$, $K_S^0K^\pm\pi^\mp$, $2(\pi^+\pi^-\pi^0)$, and $p\bar{p}$. Row (e) shows the fit to the inclusive η_c decay, while (f) denotes the background-subtracted $RM(\pi^+\pi^-\gamma)$ spectrum with the signal shape overlaid.

$E_\gamma = (m_{h_c}^2 - M^2)/2m_{h_c}$ is the energy of the transition photon, where m_{h_c} is the h_c mass [7].

$$f_{\rm d}(E_\gamma) = \frac{E_0^2}{E_\gamma E_0 + (E_\gamma - E_0)^2}$$

is the damping factor [19], where $E_0 = E_\gamma(m_{\eta_c})$ is the most probable transition energy.

$B(M)$ denotes the function which is used to describe the background shape. For exclusive decay modes, polynomial functions are used. For $\eta_c \to 2(\pi^+\pi^-\pi^0)$, the backgrounds are represented with polynomial functions of third order. For other exclusive decay modes, the backgrounds are linear functions. For the inclusive decay mode, it is a combination of the distribution from h_c sidebands and a polynomial function.

Figure 3 shows the simultaneous fit results. The fitted BFs are summarized in Table III, together with the detection efficiencies and signal yields at each energy point.

VI. CHARGED TRACK MULTIPLICITY OF η_c INCLUSIVE DECAYS

The MC simulation for the inclusive η_c decay has been introduced in Sec. III. The performance of the inclusive simulation, to some extent, can be investigated by the consistency of the charged track multiplicity [10,20,21]. Below, we introduce how to obtain the true charged track multiplicity of η_c inclusive decay. An even number of charged tracks is generated in an event due to the charge conservation, while any number of charged tracks can be observed due to the detector acceptance and reconstruction efficiency. The observed charged track multiplicity of η_c can be obtained by fitting for the η_c signal in the $\pi^+\pi^-\gamma$ recoil mass with the number of extra candidate tracks required to be 0, 1, 2, 3, $\cdots$, respectively. To obtain the charged track multiplicity at the production level, an unfolding method is employed based on an efficiency

TABLE III. Detection efficiencies (ϵ) for η_c inclusive and exclusive decays, fit results including the observed number of signal events (N_{obs}), and the fitted BFs for the four η_c exclusive decay modes. The statistical uncertainties of the observed numbers of the signal yields for the inclusive decay are obtained directly from the fit, while the numbers of signal events for the exclusive decays are calculated via Eq. (3) rather than being obtained directly from the fit, so no uncertainties are provided.

| Category				
Decay modes	$\sqrt{s}$(GeV)	ϵ (%)	N_{obs}	BF (%)
$\eta_c \to K^+ K^- \pi^0$	4.23	15.95	38.6	1.15 ± 0.12
	4.26	15.33	26.6	
	4.36	18.82	30.6	
	4.42	17.92	50.2	
	sum	$\cdots$	146.0	
$\eta_c \to K_S^0 K^\pm \pi^\mp$	4.23	17.50	66.7	2.60 ± 0.21
	4.26	19.67	53.7	
	4.36	20.67	52.8	
	4.42	21.22	93.5	
	sum	$\cdots$	266.7	
$\eta_c \to 2(\pi^+\pi^-\pi^0)$	4.23	2.93	91.9	15.2 ± 1.8
	4.26	2.60	58.6	
	4.36	3.38	71.2	
	4.42	3.07	111.6	
	sum	$\cdots$	333.3	
$\eta_c \to p\bar{p}$	4.23	34.68	8.4	0.120 ± 0.026
	4.26	37.67	7.0	
	4.36	40.00	6.9	
	4.42	40.72	12.1	
	sum	$\cdots$	34.4	
Inclusive decays	4.23	40.45	$8\,314 \pm 584$	$\cdots$
	4.26	45.17	$6\,651 \pm 499$	
	4.36	46.59	$6\,420 \pm 420$	
	4.42	46.69	$11\,083 \pm 615$	
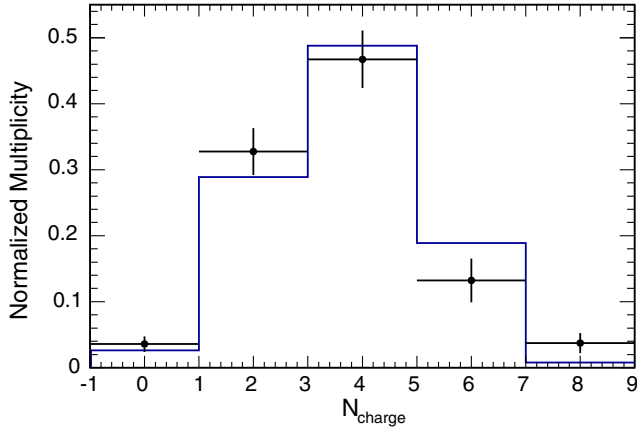
FIG. 4. Normalized distributions of charged tracks multiplicities at the production level in η_c decays, summed over all center-of-mass energies. The blue histogram represents results from MC simulation, while black dots with error bar from data. The label 8 on the axis of N_{charge} means $N_{charge} \geq 8$.

TABLE IV. The normalized multiplicity of η_c at production level with systematic uncertainties.

N_{charge}	Normalized values
0	$0.036 \pm 0.011 \pm 0.007$
2	$0.328 \pm 0.035 \pm 0.043$
4	$0.467 \pm 0.044 \pm 0.064$
6	$0.132 \pm 0.033 \pm 0.022$
≥ 8	$0.037 \pm 0.015 \pm 0.009$

matrix, whose matrix elements, ϵ_{ij}, represent the probabilities of an event generated with j tracks being observed with i tracks. The efficiency matrix is determined from the inclusive η_c MC samples. The unfolding of data is achieved by minimizing a χ^2 value, defined as

$$\chi^2 = \sum_{i=1}^{8} \frac{(N_i^{obs} - \sum_{j=0}^{8} \epsilon_{ij} \cdot N_j)^2}{(\sigma_i^{obs})^2}, \tag{5}$$

where the values $N_i^{obs}(i = 0, 1, 2, \ldots)$ are the observed multiplicities of charged tracks in the data sample, σ_i^{obs} are the corresponding uncertainties, while $N_j(j = 0, 2, 4, \ldots)$ are the true multiplicities of charged tracks at the production level in the data sample. For simplicity, the events with eight or more tracks are considered in a single value, $N_{\geq 8}$, so are the efficiencies, $\epsilon_{\geq 8}$.

Figure 4 shows the charged track multiplicity distribution of inclusive η_c decays after combining the data at the four center-of-mass energies. According to Eq. (5), the normalized numerical results are summarized in Table IV.

VII. SYSTEMATIC UNCERTAINTIES

A. Measurement of BF($\eta_c \to X$)

The systematic uncertainties on the BF measurements for exclusive η_c decays from different sources are described below and listed in Table V. The total systematic uncertainty is determined by the sum in quadrature of the individual values, assuming all sources to be independent.

1. MDC tracking and PID

The uncertainty from the tracking efficiency and PID for the two soft pions in the process $e^+ e^- \to \pi^+ \pi^- h_c$ cancels since the BFs are measured by a relative method, as mentioned in the introduction. We only consider the uncertainty from tracking efficiency and PID of the η_c decay products. The involved charged tracks are pions (not including the pions from K_S^0 decay), kaons, and protons. Their uncertainties are studied with different control samples, $e^+ e^- \to \pi^+ \pi^- K^+ K^-$ for pions and kaons, $e^+ e^- \to p\pi^- \bar{p}\pi^+$ ($e^+ e^- \to p\pi^- \bar{p}\pi^+\pi^+\pi^-$) for protons. The uncertainties from tracking efficiency are 1% for each

TABLE V. Relative systematic uncertainties (in %) in the branching fractions for the different final states of η_c decays.

Category (%)		$\eta_c \to K^+K^-\pi^0$	$\eta_c \to K_S^0 K^\pm \pi^\mp$	$\eta_c \to 2(\pi^+\pi^-\pi^0)$	$\eta_c \to p\bar{p}$
Tracking		4.0	3.0	4.0	4.0
PID		2.0	2.0	4.0	2.0
π^0 reconstruction		3.75	⋯	3.23	⋯
Kinematic Fit		0.46	0.30	1.09	0.07
K_S^0 reconstruction		⋯	1.2	⋯	⋯
MC model		0.85	0.79	1.49	0.73
h_c mass window		1.93	2.35	3.01	5.91
Fitting	fitting range	5.62	5.21	6.56	3.65
	background shape (exclusive)	0.60	0.63	5.12	8.37
	sidebands range (inclusive)	1.17	1.26	1.25	1.14
	background form (inclusive)	2.63	2.73	2.67	2.71
	Mass resolution	0.06	0.10	0.14	0.10
	resonant parameters of η_c	0.81	0.81	0.38	0.79
	damping factors	0.89	1.57	1.09	1.74
Total		9.0	7.7	11.6	12.3

pion, and 2% for each kaon or proton. The uncertainties for PID are 1% for each pion, kaon or proton.

2. π^0 reconstruction

The systematic uncertainty from π^0 reconstruction is studied with $\psi(3686) \to \pi^0\pi^0 J/\psi$ using $1.06 \times 10^8 \, \psi(3686)$ events and $e^+e^- \to \omega\pi^0 \to \pi^+\pi^-\pi^0\pi^0$ using a data sample of 2.93 fb^{-1} collected at the $\psi(3770)$ resonance. The uncertainty as a function of π^0 momentum is determined. The uncertainty from π^0 reconstruction is calculated with the function, according to the momentum distribution of the π^0 in the decays studied.

3. Kinematic fit

The systematic uncertainty from the kinematic fit is estimated by correcting the helix parameters of the charged tracks and the corresponding covariance matrix of the MC simulations to improve the agreement between data and MC simulations. The results with the corrections are taken as the final results since as the MC simulations are more consistent with the data after corrections. The detailed description can be found in Ref. [22]. The helix parameters are extracted from the control samples, $e^+e^- \to K^+K^-\pi^+\pi^-$ with data sample taken at $\sqrt{s} = 4.26$ GeV, and $J/\psi \to p\bar{p}\pi^+\pi^-$. The differences in the detection efficiency between the MC samples with and without the corrections are taken as the uncertainties due to the kinematic fit.

4. K_S^0 reconstruction

The K_S^0 reconstruction is studied with two control samples, $J/\psi \to K^{*\pm}\bar{K}^\mp$ and $J/\psi \to \phi K_S^0 K^\pm \pi^\mp$. The difference in the K_S^0 reconstruction efficiency between the MC

simulation and the data is 1.2% [23], which is taken as the uncertainty due to K_S^0 reconstruction.

5. MC model

In the MC simulation, the process $e^+e^- \to \pi^+\pi^- h_c$ is modeled with a phase space (PHSP) distribution. In fact, there is a confirmed intermediate state $Z_c(4020)$ and a potential intermediate state $Z_c(3900)$, in the $\pi^+\pi^- h_c$ final state. The uncertainty caused by the intermediate states is estimated by mixing the MC events including $Z_c(4020)/Z_c(3900)$ component according to the measured fractions [9,24]. The difference in the detection efficiency is taken as the uncertainty.

For the exclusive η_c decay modes, intermediate resonant states may affect the detection efficiency. MC samples related to η_c multibody decays are generated by sampling according to the invariant mass distributions or mixing the known intermediate states, or changing the decay model used in the MC simulation. The difference in the efficiency with and without intermediate states is taken as the uncertainty.

The uncertainty due to the inconsistency between data and MC simulation on the charged track multiplicity in inclusive η_c decays is estimated based on the multiplicity obtained by the unfolding method mentioned in Sec. VI. The detection efficiency for inclusive decay can also be recalculated with the following formula:

$$\epsilon_{\text{inclusive}} = \sum_j \left(N_j \sum_i \epsilon_{ij} \right),$$

where N_j are the normalized multiplicities in data, listed in Table IV, and ϵ_{ij} are the elements of the efficiency matrix in Eq. (5). The differences between this result and the original

TABLE VI. Systematic uncertainties (%) in the multiplicity of η_c.

Category (%)		N_0	N_2	N_4	N_6	$N_{\geq 8}$
Tracking		2.0	2.0	2.0	2.0	2.0
PID		2.0	2.0	2.0	2.0	2.0
MC model	intermediate states	4.19	3.46	5.22	7.47	7.47
	η_c inclusive decays	10.40	10.60	11.76	9.31	8.87
h_c mass window		11.70	3.54	3.01	5.91	15.26
Fit	fitting range	5.92	3.84	1.13	4.28	6.34
	background shape	8.04	3.41	1.96	8.96	11.80
	mass resolution	0.14	0.10	0.01	0.32	0.46
	resonant parameters of η_c	0.68	0.34	0.44	0.65	0.85
	damping factors	1.35	0.34	0.34	0.56	4.10
Total		19.3	13.1	13.7	16.9	23.9

one are taken into account in the simultaneous fit. It is found that the influence on $BF(\eta_c \to X)$ is negligible. This comparison also indicates that the measured N_j are reliable, since the nominal inclusive efficiency is determined by the recoil mass of the transition pions and the $E1$ photon.

6. h_c mass window

The uncertainty from the h_c mass window is estimated by randomly changing the low and high boundaries of the h_c signal region in the ranges of $[3.512, 3.518]$ GeV/c^2 and $[3.532, 3.538]$ GeV/c^2 and fitting the spectrum with efficiencies estimated in the corresponding intervals. The procedure is repeated for 800 times, and the distributions of the fitted BFs follow Gaussian functions. The obtained standard deviations are taken as the uncertainties due to the h_c mass window selection.

7. *Fit procedure*

This uncertainty arises from the fit range, the background shape, the mass resolution, the parameters of the η_c resonance, the efficiency curves, and the damping factor.

The uncertainty from the fit range is estimated by randomly changing the lower side in the range of $[2.540, 2.555]$ GeV/c^2 and higher side in $[3.200, 3.215]$ GeV/c^2 and repeating the fit for 800 times. The root mean square (rms) of the resulting distributions are taken as the systematic uncertainties from the fit range.

The uncertainty due to the assumed background shape in the exclusive modes is estimated by changing the order of the Chebychev polynomial functions. For the inclusive decay mode, the h_c sidebands need to be considered as well, whose systematic uncertainty is estimated by randomly changing the left and right margins of the lower and upper sidebands and repeating the fit. The procedure is performed 800 times. The left and right margins of the sidebands are changed in the ranges of $[3.496, 3.450]$, $[3.503, 3.507]$ GeV/c^2 and $[3.543, 3.547]$, $[3.548, 3.552]$ GeV/c^2 for the lower and upper sideband regions, respectively.

The distributions of the fitted results follow Gaussian functions, and the standard deviations are taken as the uncertainties from the h_c sidebands selection. The uncertainty from the polynomial is estimated by changing the order of the polynomial.

The discrepancy between data and MC simulation on detection resolution is estimated by a control sample, $\psi(2S) \to \pi^+\pi^- J/\psi$, $J/\psi \to \gamma\eta'$, $\eta' \to \gamma\pi^+\pi^-$. By fitting the η' signals, we can obtain the mass resolution for both data and MC simulations. We change the mass resolutions according to the result obtained from control sample to refit the $RM(\gamma\pi^+\pi^-)$. The differences on the BFs with and without changing the mass resolution are taken as the systematic uncertainties.

The η_c resonance parameters are fixed to the world average values in the fit. We change these values by $\pm 1\sigma$, and the larger difference is taken as the uncertainty.

The efficiency curves, as shown in Fig. 2, change slowly with $RM(\pi^+\pi^-\gamma)$. We find only a very small change in results when constant efficiencies are used. Therefore, the uncertainties due to efficiencies can be neglected.

The uncertainty from the damping factor is estimated by using an alternative form of the damping factor, which is used in the CLEO's published paper [25]. The differences between the results with the two forms of damping factor are taken as the systematic uncertainty.

B. Charged track multiplicity

The systematic uncertainties on the charged track multiplicity in η_c inclusive decay from different sources are described below and listed in Table VI. They are estimated in a similar way as introduced in Sec. VII A. The total systematic uncertainty is determined by the sum in quadrature of the individual values, assuming that all the sources are independent.

1. *MDC tracking and PID*

The uncertainties from MDC tracking and PID are the same as those in the measurement of $BF(\eta_c \to X)$.

TABLE VII. Measured BFs of $\eta_c \to K^+ K^- \pi^0$, $K_S^0 K^\pm \pi^\mp$, $2(\pi^+ \pi^- \pi^0)$, and $p\bar{p}$ with statistical (the first ones) and systematic (the second ones) uncertainties. The third uncertainties in the results from Ref. [6] are the systematic uncertainties due to the uncertainty of BF($\psi(3686) \to \pi^0 h_c$) × BF($h_c \to \gamma\eta_c$). The combined results from PDG are listed in the last column, among which BF($\eta_c \to K\bar{K}\pi$) is provided.

Final states	BF (%)	BF (%) from Ref. [6]	BF (%) from PDG [7]
$K^+ K^- \pi^0$	$1.15 \pm 0.12 \pm 0.10$	$1.04 \pm 0.17 \pm 0.11 \pm 0.10$	$7.3 \pm 0.5 (K\bar{K}\pi)$
$K_S^0 K^\pm \pi^\mp$	$2.60 \pm 0.21 \pm 0.20$	$2.60 \pm 0.29 \pm 0.34 \pm 0.25$	
$2(\pi^+ \pi^- \pi^0)$	$15.3 \pm 1.8 \pm 1.8$	$17.23 \pm 1.70 \pm 2.29 \pm 1.66$	17.4 ± 3.3
$p\bar{p}$	$0.120 \pm 0.026 \pm 0.015$	$0.15 \pm 0.04 \pm 0.02 \pm 0.01$	0.152 ± 0.016

2. h_c mass window

The uncertainties are estimated by changing the h_c mass window from $[3.515, 3.535]$ GeV/c^2 to $[3.518, 3.532]$ GeV/c^2 and $[3.512, 3.538]$ GeV/c^2. The largest changes on the multiplicity are taken as the uncertainty.

3. MC model

The uncertainty due to MC model mainly comes from the potential Z_c intermediate states and the simulation of the η_c inclusive decays. The uncertainty caused by the former has been introduced in Sec. VII A 5. For the latter, the simulation of the η_c inclusive decays has been mentioned in Sec. III. To estimate the uncertainty caused by this simulation, we made a comparison on the detection efficiencies with and without removing the unknown decay modes generated with LUNDCHARM. Conservatively, the corresponding difference is taken as the uncertainty caused by the simulation of η_c inclusive decays.

4. Fit

The uncertainties due to the fit to the recoil mass spectra of $\pi^+ \pi^- \gamma$ are evaluated by varying the fit range, sideband ranges, mass resolution, resonant parameters of η_c, and damping factors used in the fit, in similar ways as introduced in Sec. VII A. The spreads of the results obtained with the alternative assumptions are used to assign the systematic uncertainties.

VIII. SUMMARY

In summary, with the data samples collected at $\sqrt{s} = 4.23$, 4.26, 4.36, and 4.42 GeV, by comparing the exclusive and inclusive decays of η_c, we determine the BFs for $\eta_c \to K^+ K^- \pi^0$, $K_S^0 K^\pm \pi^\mp$, $2(\pi^+ \pi^- \pi^0)$, and $p\bar{p}$ via $e^+ e^- \to \pi^+ \pi^- h_c$, $h_c \to \gamma\eta_c$. The results are presented in Table VII; they agree with previous measurements by BESIII [6] within uncertainties, while the accuracy of these BFs is improved. With this improved accuracy, the measurements of the $M1$ transitions of $J/\psi \to \gamma\eta_c$ and $\psi(3686) \to \gamma\eta_c$ can be more precise, since such measurements provide combined results of BF($J/\psi(\psi(3686)) \to \gamma\eta_c$) × BF($\eta_c \to X$).

Moreover, the charged track multiplicity of η_c inclusive decay at production level is quantitatively presented for the first time in Table IV. The good consistency between data and MC simulation for this charged track multiplicity indicates that the current MC simulation works generally well. With this charged track multiplicity, many studies with η_c in the final state [26] are possible with higher precision than previously.

[1] C. Z. Yuan, Int. J. Mod. Phys. A **33**, 1830018 (2018).

[2] M. Ablikim *et al.* (BESIII Collaboration), Phys. Rev. Lett. **108**, 222002 (2012).

[3] K. Abe *et al.* (Belle Collaboration), Phys. Rev. Lett. **89**, 142001 (2002).

[4] K. Abe *et al.* (Belle Collaboration), Phys. Rev. D **70**, 071102 (2004).

[5] B. Aubert *et al.* (*BABAR* Collaboration), Phys. Rev. D **72**, 031101 (2005).

[6] M. Ablikim *et al.* (BESIII Collaboration), Phys. Rev. D **86**, 092009 (2012).

[7] C. Patrignani *et al.* (Particle Data Group), Chin. Phys. C **40**, 100001 (2016).

[8] M. Ablikim *et al.* (BESIII Collaboration), Chin. Phys. C **39**, 093001 (2015).

[9] M. Ablikim *et al.* (BESIII Collaboration), Phys. Rev. Lett. **111**, 242001 (2013).

[10] M. Ablikim *et al.* (BESIII Collaboration), Chin. Phys. C **37**, 063001 (2013).

[11] M. Ablikim *et al.* (BESIII Collaboration), Nucl. Instrum. Methods Phys. Res., Sect. A **614**, 345 (2010).

[12] C. H. Yu *et al.*, *Proceedings of IPAC2016, Busan, Korea* (2016), https://dx.doi.org/10.18429/JACoW-IPAC2016-TUYA01.

[13] S. Agostinelli *et al.* (GEANT4 Collaboration), Nucl. Instrum. Methods Phys. Res., Sect. A **506**, 250 (2003).

[14] S. Jadach, B. F. L. Ward, and Z. Was, Phys. Rev. D **63**, 113009 (2001); Comput. Phys. Commun. **130**, 260 (2000).

[15] D. J. Lange, Nucl. Instrum. Methods Phys. Res., Sect. A **462**, 152 (2001); R. G. Ping, Chin. Phys. C **32**, 599 (2008).

[16] J. C. Chen, G. S. Huang, X. R. Qi, D. H. Zhang, and Y. S. Zhu, Phys. Rev. D **62**, 034003 (2000); R. L. Yang, R. G. Ping, and H. Chen, Chin. Phys. Lett. **31**, 061301 (2014).

[17] E. Richter-Was, Phys. Lett. B **303**, 163 (1993).

[18] M. Xu *et al.*, Chin. Phys. C **33**, 428 (2009).

[19] V. V. Anashin *et al.*, Int. J. Mod. Phys. Conf. Ser. **02**, 188 (2011).

[20] M. Ablikim *et al.* (BESIII Collaboration), Chin. Phys. C **41**, 063001 (2017).

[21] M. Ablikim *et al.* (BESIII Collaboration), Chin. Phys. C **36**, 915 (2012).

[22] M. Ablikim *et al.* (BESIII Collaboration), Phys. Rev. D **87**, 012002 (2013).

[23] M. Ablikim *et al.* (BESIII Collaboration), Phys. Rev. D **92**, 112008 (2015).

[24] M. Ablikim *et al.* (BESIII Collaboration), Phys. Rev. Lett. **119**, 072001 (2017).

[25] R. E. Mitchell *et al.* (CLEO Collaboration), Phys. Rev. Lett. **102**, 011801 (2009).

[26] Z. Sun, X.-G. Wu, Y. Ma, and S. J. Brodsky, Phys. Rev. D **98**, 094001 (2018).